Vibronic Couplings in C_{60} Derivatives for Organic Photovoltaics

Tohru Sato[a,*], Naoya Iwahara[a], Kazuyoshi Tanaka[a], Hironori Kaji[b]

[a] *Department of Molecular Engineering, Graduate School of Engineering, Kyoto University, Nishikyo-ku, Kyoto 615-8510, Japan*
[b] *Institute for Chemical Research, Kyoto University, Gokasho, Uji, Kyoto 611-0011, Japan*

Abstract

Vibronic coupling constants (VCC) and reorganization energy of C_{60} derivative anions including [6,6]-phenyl-C_{61}-butyric acid methyl ester (PCBM) are evaluated. The results are analyzed in terms of the vibronic coupling density (VCD). All the molecules calculated exhibit almost the same VCCs in C_{60}^{-}. A low symmetry derivative with a delocalized LUMO over the molecule would exhibit large VCCs and not be suitable for a organic photovoltaics material from view of vibronic couplings.

1. Introduction

Fullerene derivatives have been employed as acceptors or electron-transporting materials in organic photovoltaics (OPV) [1, 2], model systems for the artificial photosynthesis [3], and so on. In these investigations, vibronic coupling (VC) or vibrational reorganization energy [4, 5, 6] plays an important role. In the carrier-transporting process, the VC gives rise to the inelastic scattering of a carrier and power loss [7]. Thus small VCs and reorganizations

*Tel: +81-75-383-2803. Fax: +81-75-383-2556. E-mail: tsato@scl.kyoto-u.ac.jp.

are desired in the process. Small vibrational reorganization energy is also required to make artificial photosynthetic models [8, 9, 3].

The reorganization energies have been evaluated in some systems such as porphyrin-fullerene dyads and donor:PCBM blends where PCBM is [6,6]-phenyl-C_{61}-butyric acid methyl ester [8, 9, 10, 11]. Experimentally, the reorganization energies have been estimated from the Stokes shift of emission spectra from the charge-transferred state [8, 9, 10]. The vibrational reorganization energies were obtained theoretically from the difference of the total energies of neutral and charge-transferred states [11]. However, the VCs in C_{60} derivative has not understood clearly, and insight into the VCs from the view of the electronic and vibrational structures is useful.

Recently we have estimated the vibronic coupling constants (VCC) of C_{60}^- from the photoelectron spectrum in gas phase [12] using the exact diagonalization of a dynamic Jahn-Teller Hamiltonian [13]. Furthermore the estimated VCCs agree well with the density functional theory calculation[13]. Therefore, the method of calculation can be applied for accurate estimations of the VCCs in C_{60} derivatives.

The VCCs can be analyzed in terms of vibronic coupling density (VCD) [14, 6]. The VCD provides a local picture of the VC from the electronic and vibrational structures, and the VCD demonstrates the strengths of the VCs of C_{60} monoanion [15]. Moreover, using the VCD analysis, we have succeeded in designing novel hole- and electron-transporting molecules with small VCCs [16, 17].

In this study, we calculate the VCCs or reorganization energies in C_{60} derivative anions (see Fig. 1) and compare the VCs with those in C_{60} anion.

As C_{60} derivatives, we treat PCBM (Fig. 1, **1**) and fullerene pyrrolidines (Figs. 1, **2** and **3**). The former is employed as an acceptor in organic thin film solar cells [1] and the latters are used as acceptors in donor-acceptor dyads [3, 9]. The calculated results are analyzed in terms of vibronic coupling density analysis.

2. Theory

Vibronic coupling constant (VCC) [4, 5, 6] for a vibrational mode α is defined by

$$V_\alpha = \left\langle \Psi(\mathbf{R_0}, \mathbf{r}) \left| \left(\frac{\partial \hat{H}(\mathbf{Q}, \mathbf{r})}{\partial Q_\alpha} \right)_{\mathbf{R_0}} \right| \Psi(\mathbf{R_0}, \mathbf{r}) \right\rangle, \tag{1}$$

where Ψ denotes the electronic wavefunction for the anionic state at the equilibrium structure of the neutral state $\mathbf{R_0}$, $\mathbf{r} = (\mathbf{r}_1, \cdots, \mathbf{r}_i, \cdots, \mathbf{r}_N)$ a set of the electron coordinates, $\hat{H}$ molecular Hamiltonian, and $\mathbf{Q} = (Q_1, \cdots, Q_\alpha, \cdots)$ a set of the normal coordinate Q_α. The direction of mode α is defined so as V_α is negative. Vibronic Hamiltonian can be written as

$$\hat{H}_{\text{vibro}} = E_0 + \sum_{\alpha}^{3M-6} \left(-|V_\alpha| Q_\alpha + \frac{1}{2}\omega_\alpha^2 Q_\alpha^2 \right), \tag{2}$$

where E_0 is the ground-state electronic energy of the anion at $\mathbf{R}_0$. The vibronic Hamiltonian can be rewritten as

$$\hat{H}_{\text{vibro}} = E_0 + \sum_{\alpha}^{3M-6} \left[\frac{1}{2}\omega_\alpha^2 \left(Q_\alpha - \frac{|V_\alpha|}{\omega_\alpha^2} \right)^2 - \frac{V_\alpha^2}{2\omega_\alpha^2} \right]. \tag{3}$$

From Eq.(3), reorganization energy for mode α is obtained as

$$E_{R,\alpha} = \frac{V_\alpha^2}{2\omega_\alpha^2}. \tag{4}$$

Total reorganization energy is calculated from

$$E_R = \sum_{\alpha} E_{R,\alpha}. \tag{5}$$

VCD for a vibrational mode α is defined by [14, 6]

$$\eta_\alpha(\mathbf{r}_i) = \Delta\rho(\mathbf{r}_i) \times v_\alpha(\mathbf{r}_i), \tag{6}$$

where $\Delta\rho(\mathbf{r}_i) = \rho(\mathbf{r}_i) - \rho_0(\mathbf{r}_i)$ is the electron density difference between the anionic density ρ and the neutral density ρ_0. Potential derivative $v_\alpha(\mathbf{r}_i)$ is defined using the nuclear attraction potential acting on a single electron:

$$u(\mathbf{r}_i) = \sum_{A=1}^{M} -\frac{Z_A e^2}{4\pi\epsilon_0 |\mathbf{r}_i - \mathbf{R}_A|}, \tag{7}$$

where M is the number of the nuclei, ϵ_0 is the electric constant, and $\mathbf{R}_A$ and Z_A denote the position and the charge of nucleus A, respectively. The potential derivative is defined by

$$v_\alpha(\mathbf{r}_i) = \left(\frac{\partial u(\mathbf{r}_i)}{\partial Q_\alpha} \right)_{\mathbf{R}_0}, \tag{8}$$

The space integral of a vibronic coupling density η_α yields the VCC:

$$V_\alpha = \int \eta_\alpha(\mathbf{r}_i)\, d^3\mathbf{r}_i = \int \Delta\rho(\mathbf{r}_i) \times v_\alpha(\mathbf{r}_i)\, d^3\mathbf{r}_i. \tag{9}$$

The VCC can be analyzed in terms of the electronic structure $\Delta\rho$ and the vibrational structure v_α through the VCD η_α based on Eq. (9). Note that a VCD is sometimes canceled in a certain region since a VCD distributes with positive and negative values [7].

Effective mode with the VCC

$$V_{\text{eff}} = \sqrt{\sum_{\alpha} V_\alpha^2} \tag{10}$$

is defined by

$$\mathbf{u}_{\rm eff} = \sum_{\alpha=1}^{3M-6} \left(\frac{|V_\alpha|}{V_{\rm eff}} \right) \mathbf{u}_\alpha, \tag{11}$$

where $\mathbf{u}_\alpha$ is a vibrational vector of mode α. For the effective mode, the frequency and the reorganization energy are

$$\omega_{\rm eff}^2 = \sum_\alpha \frac{V_\alpha^2 \omega_\alpha^2}{V_{\rm eff}^2}, \tag{12}$$

$$E_{\rm eff} = \frac{V_{\rm eff}^2}{2\omega_{\rm eff}^2}, \tag{13}$$

respectively.

3. Method of calculation

We employed the B3LYP functional with the 6-311G(d,p) basis set. The reference structures were obtained by geometry optimizations of the neutral states. Vibrational analyses were applied for the optimized structures to be checked if the structure is a stationary minimum. Analytical force calculations were performed for the optimized structures of the neutral states. We employed the Gaussian 09 packages for the optimizations, vibrational analysis, and force calculations [18]. The VCCs were evaluated using the results of the force calculations. The VCD analyses were performed using the electronic wavefunctions of the neutral and anionic states at their reference geometry as well as the vibrational modes. The VCC and VCD calculations were performed using our codes. In order to analyze the electronic structures, we performed the fragment molecular orbital (FMO) analysis using the YAeHMOP program [19, 20].

4. Results and discussion

4.1. Vibronic coupling constants and reorganization energies

Figure 2 shows the calculated vibronic coupling constants V_α (1) of C_{60}^- [13] and the anions of C_{60} derivatives (Fig 1). Since the symmetry of C_{60} is I_h, and the LUMOs belong to the t_{1u} irreducible representation, the electronic state of C_{60}^- is T_{1u}. The T_{1u} electronic state couples with a_g and h_g modes from the selection rule, $[T_{1u}^2] = a_g \oplus h_g$. C_{60} has two a_g modes and eight sets of h_g modes, and thus it has 42 active modes. For C_{60}^-, the VCCs of the $a_g(2)$ (1492 cm^{-1}), $h_g(7)$ (1442 cm^{-1}), and $h_g(8)$ (1608 cm^{-1}) modes are strong [13].

The VCCs of the derivatives are quite similar to those of C_{60}^- except for the number of active modes. The symmetries of the derivatives are lower than that of C_{60}, and hence the derivatives have larger number of active modes than C_{60} does. For example, since PCBM (Fig. 1, **1**) is C_1, all of the 258 vibrational modes are active. Among the active modes of derivatives, the modes originating from the $a_g(2)$ mode of C_{60} is the most intense, and the mode from the $h_g(8)$ mode of C_{60} is the second strongest. On the other hand, the VCCs for the modes which do not originate from the active modes of C_{60}^-, the a_g and h_g modes, are weak.

Reorganization energies $E_{R,\alpha}$ (4) are shown in Fig. 3, and total reorganization energies E_R (5) are tabulated in Table 1. The reorganization energies of the derivatives are close to that of C_{60}^-. The reorganization energy of PCBM which has the largest number of active modes is the largest among the systems. Nonetheless the difference in E_R is only 7 meV. Present reorganization energies of *ca.* 70 meV were obtained smaller than experimental

value of *ca.* 100 meV [8]. This is because the experimental value includes E_R of the donor part as well as E_R of the acceptor.

The frequencies (12), VCCs (10), and total reorganization energies (13) for the effective modes of the derivatives are almost the same as C_{60} as tabulated in Table 1. Moreover, the Mulliken charges on the substituent group are small. These results indicate that the vibronic couplings in the derivatives originate from the coupling in C_{60}.

4.2. Vibronic coupling density

Figure 4 shows the LUMO and the electron density difference $\Delta\rho$ of PCBM. In Fig. 4, white and the blue areas indicate positive and negative values, respectively. The LUMO (Fig. 4 (a)) is almost completely localized on the C_{60} fragment. The distribution of the electron density difference $\Delta\rho$ (Fig. 4 (b)) is similar to the LUMO density. However, $\Delta\rho$ appears not only on C_{60} but also on the substituent (Fig. 4 (b)). The charge transfer from C_{60} cage to the substituent (see Mulliken charge in Table 1), though small, gives rise to the change of the distribution of the electron density, and consequently $\Delta\rho$ appears on the substituent. In addition, negative polarization of $\Delta\rho$ is found on the C_{60} cage because of the Coulomb interactions between electron in doubly occupied orbitals and an additional electron in the anion. In other words, the many-body effect strongly affects $\Delta\rho$, and therefore, VCCs [21].

Since the electron density difference $\Delta\rho$ is mainly localized on the C_{60} cage, $\Delta\rho$ of the derivative anions strongly couple to vibrational modes corresponding to the $a_g(2)$ and the $h_g(8)$ modes of C_{60}. Therefore the potential derivative v_α (8) for the effective mode is localized on the C_{60} fragment (Fig. 5 (a)), and the distributions of the VCD (6) in the PCBM anion (Fig. 5 (b))

is similar to that of C_{60}^- [15]. Furthermore, the effective mode of the PCBM anion is the stretching mode of the 6:6 C=C double bond, which is the same as in C_{60}^- [22]. Similar discussion holds for the C_{60} derivative anions other than PCBM.

4.3. Fragment molecular orbital analysis

The VCCs or reorganization energies of C_{60}^- and the derivatives are close to each other because the distribution of the LUMOs of the derivatives are similar to that of C_{60}. This conservation of LUMO can be explained based on the fragment molecular orbital (FMO) analysis. For the analysis, each C_{60} derivative is divided into C_{60} (Fragment A) and the substituted group (Fragment B). The FMO of PCBM is shown in Fig. 6. The HOMO of PCBM consists of the h_u and the t_{1u} frontier orbitals of C_{60} fragment (Frag. A) and the LUMO of the substituent (Frag. B). One of the t_{1u} LUMOs contributes to the HOMO of PCBM, while the others do not. The latter orbitals are almost unchanged under the addition of the substituent. Therefore, the LUMO of PCBM is almost the same as one of the LUMOs of C_{60}.

5. Summary

VCCs and reorganization energy of C_{60} derivative anions including PCBM were evaluated. The results were analyzed in terms of the VCD. All the molecules calculated exhibit almost the same VCCs in C_{60}^-. Since the LUMO of the derivatives originate from the t_{1u} LUMO, $\Delta\rho$ is localized on the C_{60} fragment. This result indicates that the electronic structure of C_{60} is robust and kept in the C_{60} derivatives. The reorganization energy of PCBM is slightly larger than that of C_{60}. This is because the molecular symmetry of

PCBM is low. In order to avoid increase of the reorganization energy, (1) $\Delta\rho$ should localize on the C_{60} fragment, and (2) the molecular symmetry should be high. Therefore, a low symmetry derivative with a delocalized LUMO would exhibit large VCCs and not be suitable for a OPV material or model system of photosynthesis from view of vibronic couplings.

Acknowledgement

Numerical calculations were performed partly in the Supercomputer Laboratory of Kyoto University and Research Center for Computational Science, Okazaki, Japan. This work was also supported in part by the Global COE Program "International Center for Integrated Research and Advanced Education in Materials Science" (No. B–09) of the Ministry of Education, Culture, Sports, Science and Technology (MEXT) of Japan, administrated by the Japan Society for the Promotion of Science.

References

[1] G. Yu, J. Gao, J. C. Hummelen, F. Wudl, A. J. Heeger, Science 270 (1995) 1789.

[2] B. C. Thompson, J. M. J. Fréchet, Angew. Chem. Int. Ed. 47 (2008) 58.

[3] H. Imahori, Bull. Chem. Soc. Jpn. 80 (2007) 621.

[4] I. B. Bersuker, V. Z. Polinger, Vibronic Interactions in Molecules and Crystals, Springer–Verlag, Berlin and Heidelberg, 1989.

[5] I. B. Bersuker, The Jahn–Teller Effect, Cambridge University Press, Cambridge, 2005.

[6] T. Sato, K. Tokunaga, N. Iwahara, K. Shizu, K. Tanaka, in: H. Köppel, D. R. Yarkony, H. Barentzen (Eds.), The Jahn–Teller Effect: Fundamentals and Implications for Physics and Chemistry, Springer–Verlag, Berlin, 2009, p. 99.

[7] T. Sato, K. Shizu, T. Kuga, K. Tanaka, H. Kaji, Chem. Phys. Lett. 458 (2008) 152–156.

[8] H. Imahori, N. V. Tkachenko, V. Vehmanen, K. Tamaki, H. Lemmetyinen, Y. Sakata, S. Fukuzumi, J. Phys. Chem. A 105 (2001) 1750.

[9] H. Imahori, H. Yamada, D. M. Guldi, Y. Endo, A. Shimomura, S. Kundu, K. Yamada, T. Okada, Y. Sakata, S. Fukuzumi, Angew. Chem. Int. Ed. 41 (2002) 2344.

[10] K. Vandewal, K. Tvingstedt, A. Gadisa, O. Inganäs, J. M. Manca, Phys. Rev. B 81 (2010) 125204.

[11] T. Liu, A. Troisi, J. Phys. Chem. C 115 (2011) 2406.

[12] X. B. Wang, H. K. Woo, L. S. Wang, J. Chem. Phys. 123 (2005) 051106.

[13] N. Iwahara, T. Sato, K. Tanaka, L. F. Chibotaru, Phys. Rev. B 82 (2010) 245409.

[14] T. Sato, K. Tokunaga, K. Tanaka, J. Phys. Chem. A 112 (2008) 758.

[15] N. Iwahara, T. Sato, K. TanakaSubmitted.

[16] K. Shizu, T. Sato, K. Tanaka, H. Kaji, Appl. Phys. Lett. 97 (2010) 142111.

[17] K. Shizu, T. Sato, A. Ito, K. Tanaka, H. Kaji, J. Mater. Chem. 21 (2011) 6375.

[18] M. J. Frisch, G. W. Trucks, H. B. Schlegel, G. E. Scuseria, M. A. Robb, J. R. Cheeseman, G. Scalmani, V. Barone, B. Mennucci, G. A. Petersson, H. Nakatsuji, M. Caricato, X. Li, H. P. Hratchian, A. F. Izmaylov, J. Bloino, G. Zheng, J. L. Sonnenberg, M. Hada, M. Ehara, K. Toyota, R. Fukuda, J. Hasegawa, M. Ishida, T. Nakajima, Y. Honda, O. Kitao, H. Nakai, T. Vreven, J. A. Montgomery, Jr., J. E. Peralta, F. Ogliaro, M. Bearpark, J. J. Heyd, E. Brothers, K. N. Kudin, V. N. Staroverov, R. Kobayashi, J. Normand, K. Raghavachari, A. Rendell, J. C. Burant, S. S. Iyengar, J. Tomasi, M. Cossi, N. Rega, J. M. Millam, M. Klene, J. E. Knox, J. B. Cross, V. Bakken, C. Adamo, J. Jaramillo, R. Gomperts, R. E. Stratmann, O. Yazyev, A. J. Austin, R. Cammi, C. Pomelli, J. W. Ochterski, R. L. Martin, K. Morokuma, V. G. Zakrzewski, G. A. Voth, P. Salvador, J. J. Dannenberg, S. Dapprich, A. D. Daniels, O. Farkas, J. B. Foresman, J. V. Ortiz, J. Cioslowski, D. J. Fox, Gaussian 09 Revision B.1, gaussian Inc. Wallingford CT 2009.

[19] G.A.Landrum and W.V.Glassey, bind (ver 3.0). bind is distributed as part of the YAeHMOP extended Hückel molecular orbital package and is freely available on the WWW at; http://sourceforge.net/projects/yaehmop/.

[20] G.A.Landrum, viewkel (ver 3.0). viewkel is distributed as part of the YAeHMOP extended Hückel molecular orbital package and is freely available on the WWW at; http://sourceforge.net/projects/yaehmop/.

[21] T. Sato, K. Shizu, K. Uegaito, N. Iwahara, K. Tanaka, H. Kaji, Chem. Phys. Lett. 507 (2011) 151.

[22] T. Sato, N. Iwahara, N. Haruta, K. Tanaka, Chem. Phys. Lett.doi:10.1016/j.cplett.2012.02.025.

Table 1: Total reorganization energies E_R (meV). Frequencies ω_{eff} (cm^{-1}, vibronic couplings V_{eff} (10^{-4} a.u.), and stabilization energies E_{eff} (meV) of the effective modes. Sums of Mulliken charges on the substituent groups.

	E_R	ω_{eff}	V_{eff}	E_{eff}	Charge
C_{60}^-	67.2	1450	4.01	50.1	
$\mathbf{1}^-$	74.0	1452	4.03	50.4	-0.098
$\mathbf{2}^-$	69.2	1466	4.00	48.8	-0.095
$\mathbf{3}^-$	69.1	1460	4.00	49.1	-0.109

Figure Captions

Figure 1: Calculated C_{60} derivatives. **1** is the [6,6]-phenyl-C-61-butyric acid methyl ester (PCBM), **2** is the fullerene pyrrolidine, and **3** is a fullerene pyrrolidine derivative.

Figure 2: Vibronic coupling constants of (a) C_{60}^{-}, (b) $\mathbf{1}^{-}$, (c) $\mathbf{2}^{-}$ (C_s), and (d) $\mathbf{3}^{-}$ (C_1) in 10^{-4} a.u.

Figure 3: Reorganization energies $E_{R,\alpha}$ of (a) C_{60}^{-}, (b) $\mathbf{1}^{-}$, (c) $\mathbf{2}^{-}$, and (d) $\mathbf{3}^{-}$ in meV.

Figure 4: (a) LUMO (isosurface value=0.025 a.u.) and (b) $\Delta\rho$ (isosurface value=0.001 a.u.) of **1** (PCBM).

Figure 5: (a) v_{eff} (isosurface value=0.005 a.u.) and (b) η_{eff} (isosurface value=5×10^{-6} a.u.) for the effective mode in PCBM.

Figure 6: FMO analysis for **1** (PCBM). Threshold of the MO is 0.03 a.u. for the system and fragment A and 0.05 a.u. for the fragment B.

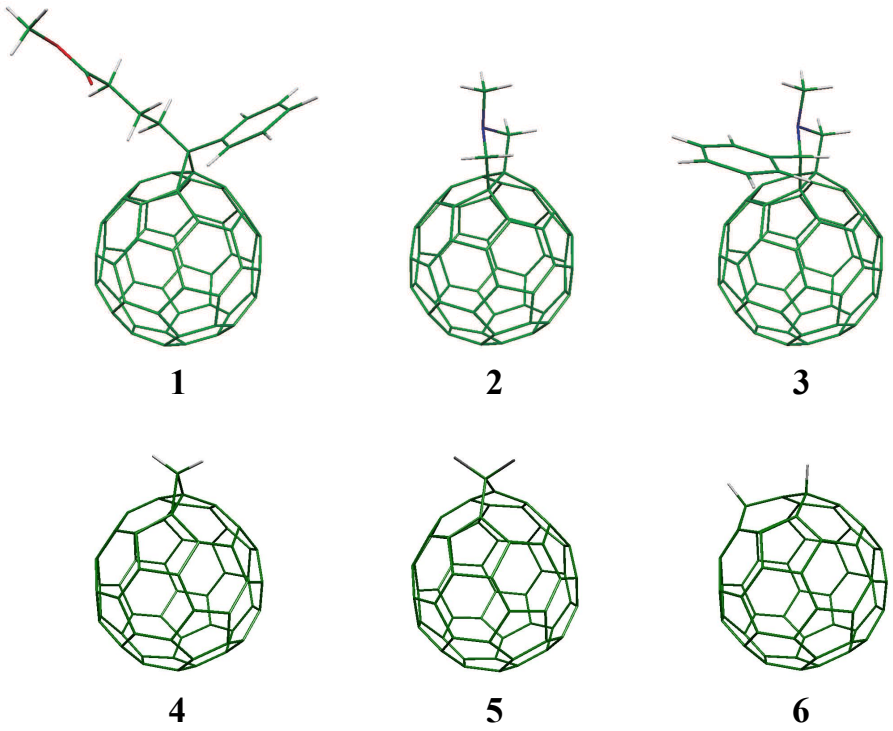

Figure 1: Sato *et al.*

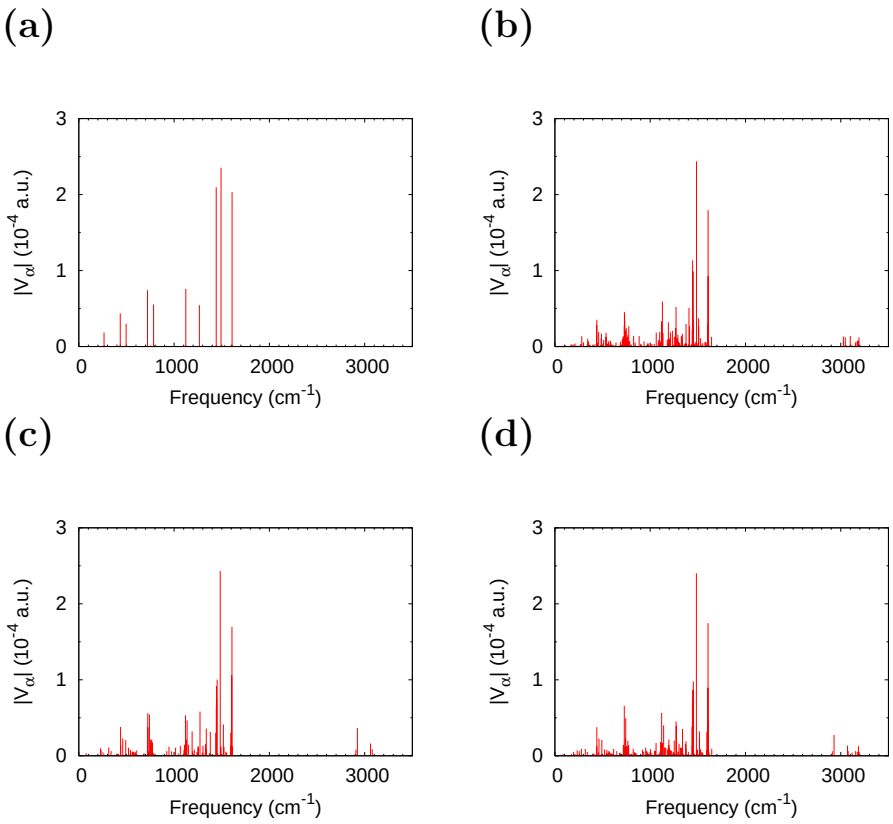

Figure 2: Sato *et al.*

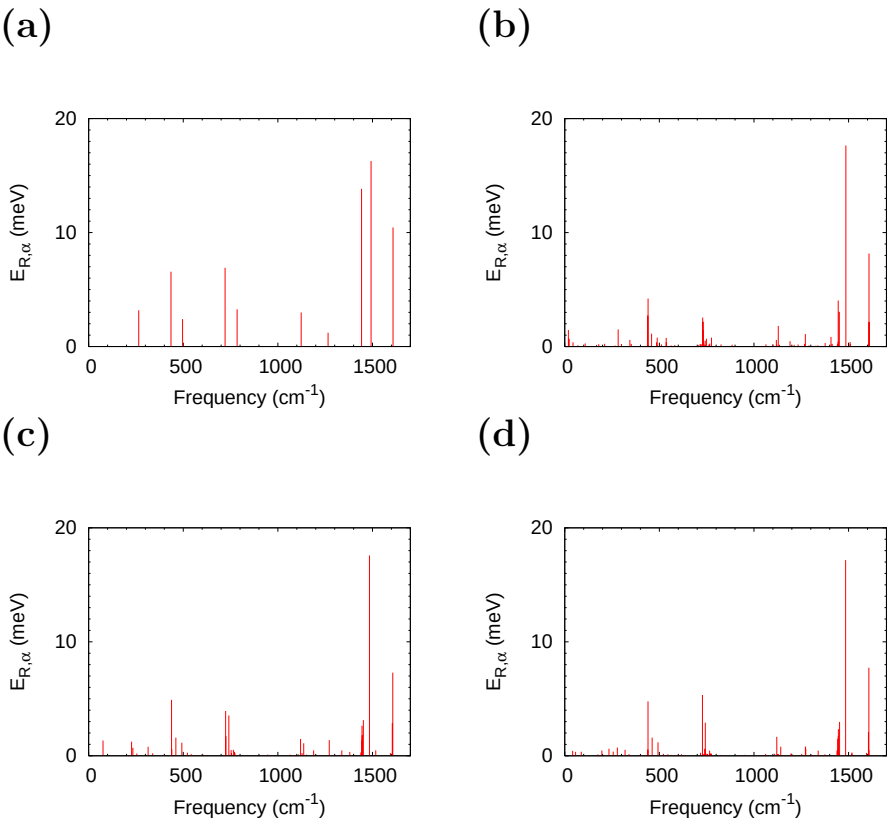

Figure 3: Reorganization energies $E_{R,\alpha}$ of (a) C_{60}^{-}, (b) $PCBM^{-}$, (c) C_{60} pyrrolidine^{-}, and (d) C_{60} pyrrolidine derivative^{-} in meV.

(a) LUMO

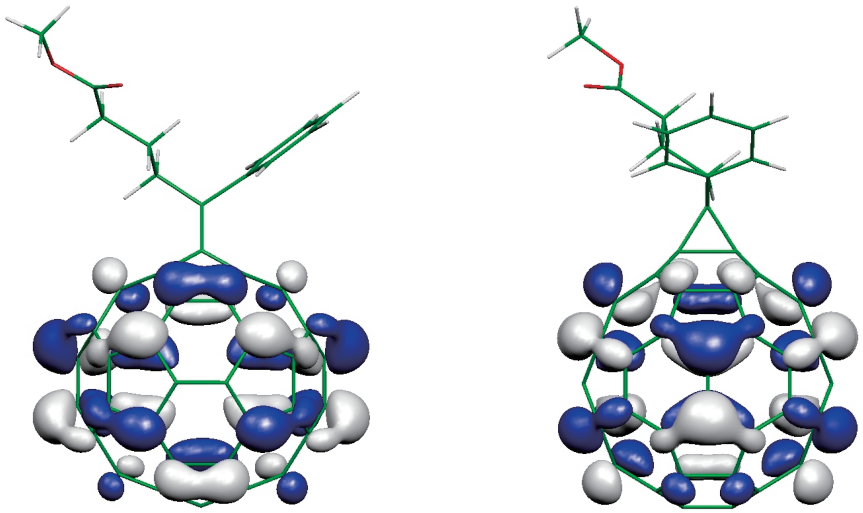

(b) $\Delta\rho$

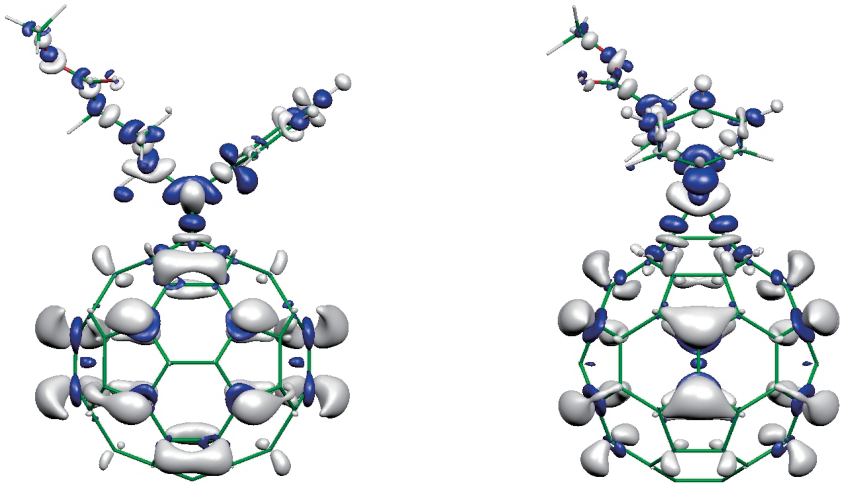

x y

Figure 4: Sato *et al.*

(a) v_{eff}

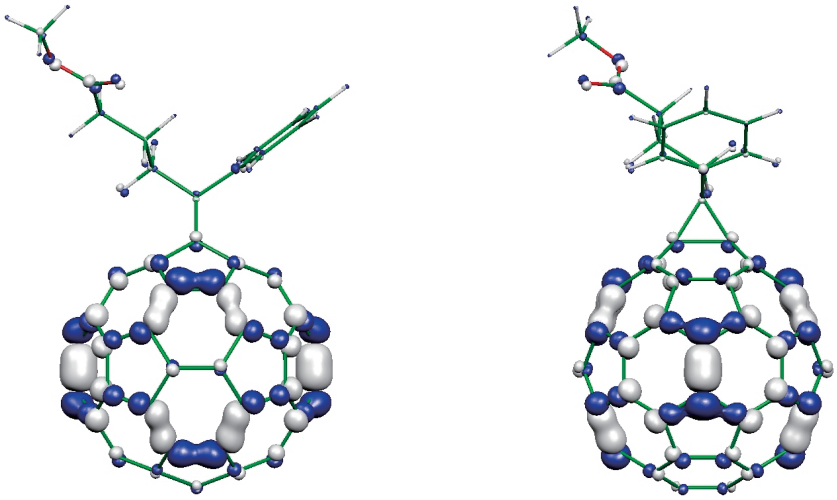

(b) η_{eff}

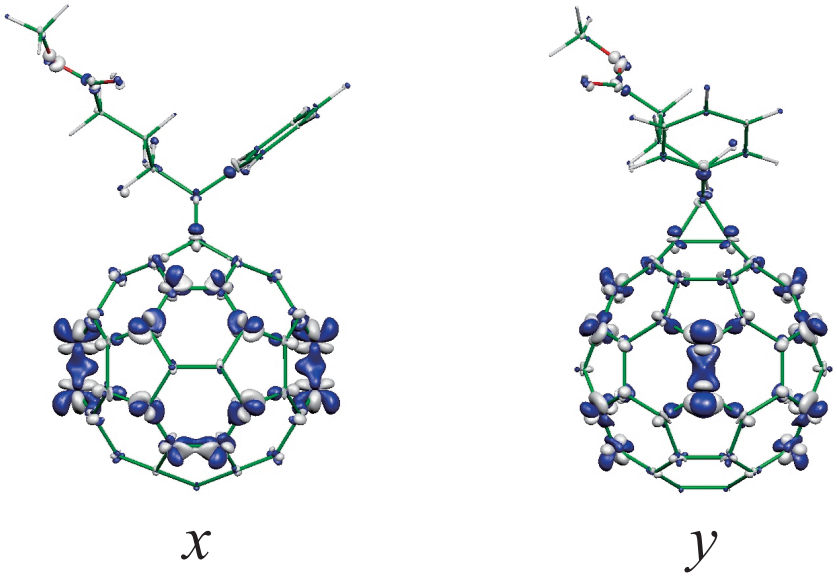

Figure 5: Sato *et al.*

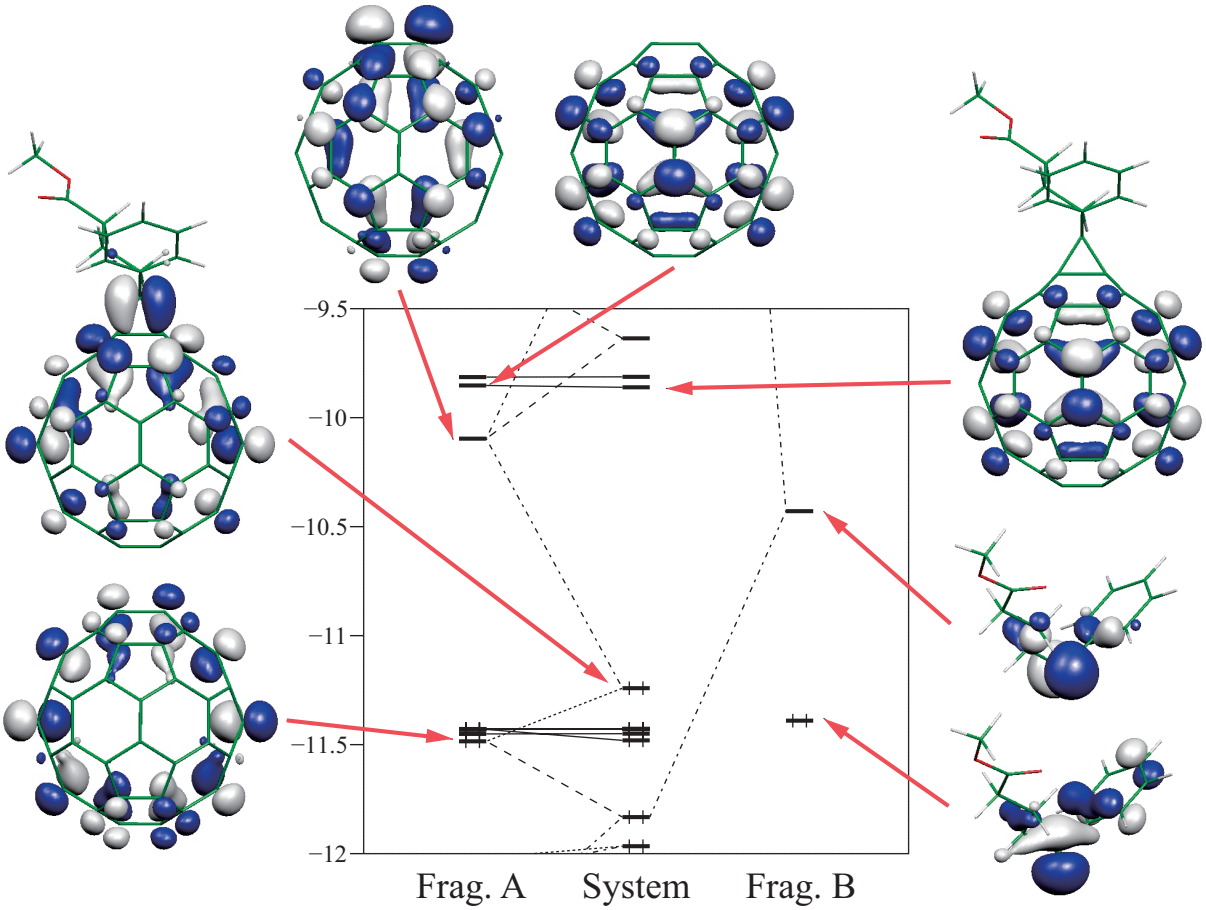

Figure 6: Sato *et al.*